# Micromechanical Modelling of Interfacial Debonding in AA1100/Graphite Nanoparticulate Reinforced Metal Matrix Composites

**A. Chennakesava Reddy**

Assistant Professor, Department of Mechanical Engineering, MJ College of Engineering and Technology, Hyderabad, India
dr_acreddy@yahoo.com

**Abstract:** A square array unit cell/spherical particle RVE models were employed to evaluate interfacial debonding using cohesive zone analysis. The particulate metal matrix composites are graphite/AA1100 alloy at volume fractions of 10%, 20% and 30% graphite. Interface debonding was observed in all the composites. In addition to interfacial debonding, the graphite nanoparticle experiences high stress due to load transfer from the matrix.

**Keywords:** AA1100 alloy, graphite, spherical particle, RVE model, finite element analysis, interface debonding.

## 1. INTRODUCTION

Interfaces between ceramic and metallic phases are prominent features in many technologically important composite materials, and understanding their structure and properties is therefore of considerable interest. The continuum models based on the classical plasticity theories could explain the load transfer effect from the composite matrix to the reinforcing particle and successfully predict the plastic work hardening behavior of the particulate metal matrix composites depending on the particle volume fraction [1]. Cohesive interactions are generally a function of displacement jump (or separation). If the displacement jump is greater than a characteristic length ($\delta_n$), complete failure occurs (i.e., no load bearing capacity). Non-potential based cohesive interaction models are relatively simple to develop, because a symmetric system is not required [2]. However, these models do not guarantee consistency of the constitutive relationship for arbitrary mixed-mode conditions, because they do not account for all possible separation paths. For potential-based models, the traction-separation relationships across fracture surfaces are obtained from a potential function, which characterizes the fracture behavior [3]. The cohesive zone model with the finite element method (FEM) was implemented for the analysis of several combinations of reinforcement particles and matrix alloys [4-17].

In the present work, an axisymmetric unit cell model containing three zones with a perfect particle/matrix interface (through cohesive zone model) is employed to represent the representative cell of the graphite nanoparticle reinforced AA1100 alloy matrix composite with a diamond array of spherical particles as shown in figure 1.

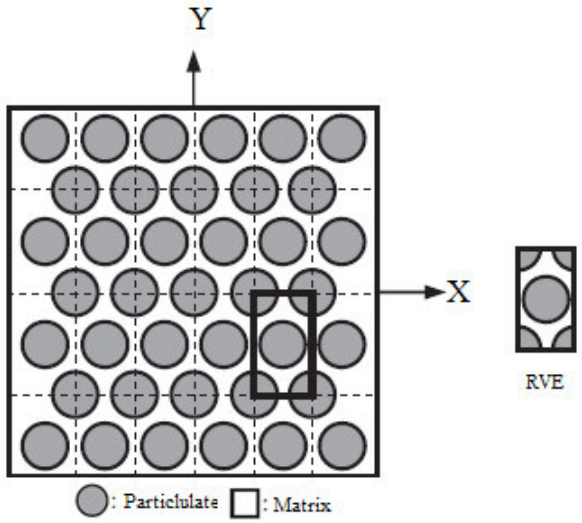


**Figure 1:** The RVE model.

## 2. MATERIALS AND METHODS

The computational domains consist of various volume fractions (10%, 20%, and 30%) of graphite nanoparticles reinforced in AA1100 alloy matrix. Initially, both AA1100 alloy matrix and graphite nanoparticle were kept in contact with zero separation distance. PLANE183 element was used to model the matrix and the nanoparticles. The cohesive zone can be incorporated in the continuum formulation by applying the cohesive tractions as boundary conditions. The cohesive element is implemented as a linear element with four nodes. The finite element analysis was carried out for the single inclusion model undergoing a tensile load. The elastic material properties are given by $E_m$ = 68.90 GPa, $E_p$ = 445 GPa, $\nu_m$ = 0.33 and $\nu_p$ = 0.19.

The stress distribution in the particulate is determined by relating shear strains in the matrix around the particulate to the macroscopic strain of the composite as follows:

$$\sigma_p = E_p \varepsilon_c [1 - cosh(nx/r) sech(ns)] \quad (1)$$

where $\varepsilon_c$ is the composite strain, $s$ is the particulate aspect ratio (length/diameter) and $n$ is a dimensionless constant given by:

$$n = \left[\frac{2E_m}{E_p(1+\nu_m) ln(1+\nu_p)}\right]^{1/2} \quad (2)$$

in which $\nu_m$ is the Poisson ratio of the matrix. The variation of interfacial shear stress along the particulate length is derived as follows:

$$\tau_i = \frac{n\varepsilon_c}{2} E_p sinh\left(\frac{nx}{r}\right) sech(ns) \quad (3)$$

The equation for the stress in the particulate, together with the assumption of a average tensile strain in the matrix equal to that imposed on the composite, can be used to evaluate the composite stiffness. This leads to:

$$\sigma_c = \varepsilon_c \left[\nu_p E_p \left(1 - \frac{tanh(ns)}{ns}\right) + (1 - \nu_p) E_m\right] \quad (4)$$

The expression in square brackets is the composite stiffness. The stiffness is a function of particulate aspect ratio, particulate/matrix stiffness ratio and particulate volume fraction.

If the particle deforms in an elastic manner (according to Hooke's law) then,

$$\tau = \frac{n}{2}\sigma_p \quad (5)$$

If interfacial debonding/yielding is considered to occur when the interfacial shear stress reaches its shear strength

$$\tau = \tau_{max} \quad (6)$$

For particle/matrix interfacial fracture can be established whereby,

$$\tau_{max} < \frac{n\sigma_p}{2} \quad (7)$$

This approach suggests that the outcome of a matrix crack impinging on an embedded particle depends on the balance between the particle strength and the shear strength of the interface. For plane strain conditions, the macro stress- macro strain relation is as follows:

$$\begin{Bmatrix} \overline{\sigma_x} \\ \overline{\sigma_y} \\ \overline{\tau_{xy}} \end{Bmatrix} = \begin{bmatrix} \overline{C_{11}} & \overline{C_{12}} & 0 \\ \overline{C_{21}} & \overline{C_{22}} & 0 \\ 0 & 0 & \overline{C_{33}} \end{bmatrix} \times \begin{Bmatrix} \overline{\varepsilon_x} \\ \overline{\varepsilon_y} \\ \overline{\gamma_{xy}} \end{Bmatrix} \quad (8)$$

The interfacial tractions can be obtained by transforming the micro stresses at the interface as given in Eq. (3):

$$t = \begin{Bmatrix} t_z \\ t_n \\ t_t \end{Bmatrix} = T\sigma \quad (9)$$

where, $T = \begin{bmatrix} 0 & 0 & 0 \\ cos^2\theta & sin^2\theta & 2sin\theta cos\theta \\ -sin\theta cos\theta & sin\theta cos\theta & cos^2\theta - sin^2\theta \end{bmatrix}$

## 1. RESULTS AND DISCUSSION

The tensile modulus increases with volume fraction of graphite nanoparticles as shown figure 2a. The shear modulus decreases with increase in the volume fraction of graphite nanoparticles in the composites (figure 2b). The major Poisson's ratio increases with volume fraction of graphite nanoparticles. The stiffness mismatch between graphite nanoparticles and AA1100 alloy matrix is 376.10 GPa. The condition $\tau_{max} < n\sigma_p/2$ is satisfied for the incidence of debonding in the composites including 10%, 20% and 30% graphite nanoparticles (figure 3). The strain energy density developed at the interface is higher than that developed in graphite nanoparticle and AA1100 alloy matrix (figure 4). The strain energy density decreases with increase in the volume fraction of graphite nanoparticles (figures 4 and 5).

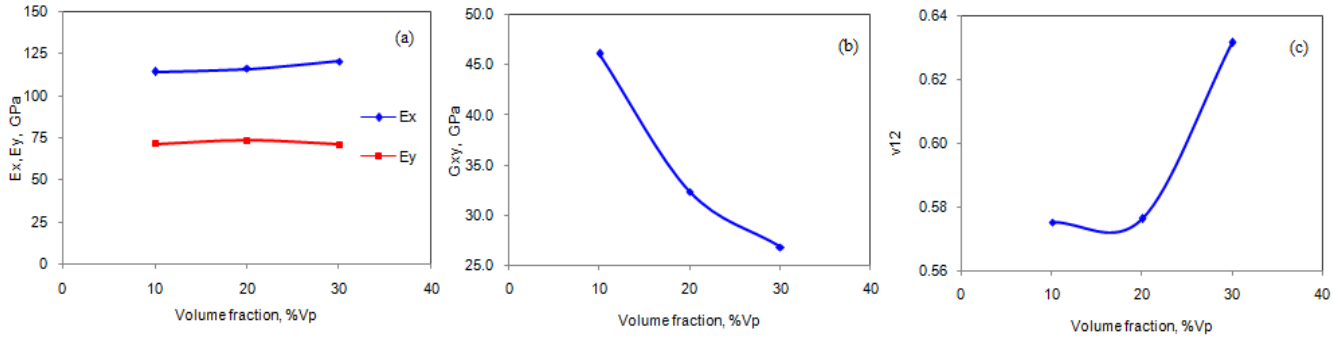


**Figure 2:** Effect of volume fraction on effective material properties.

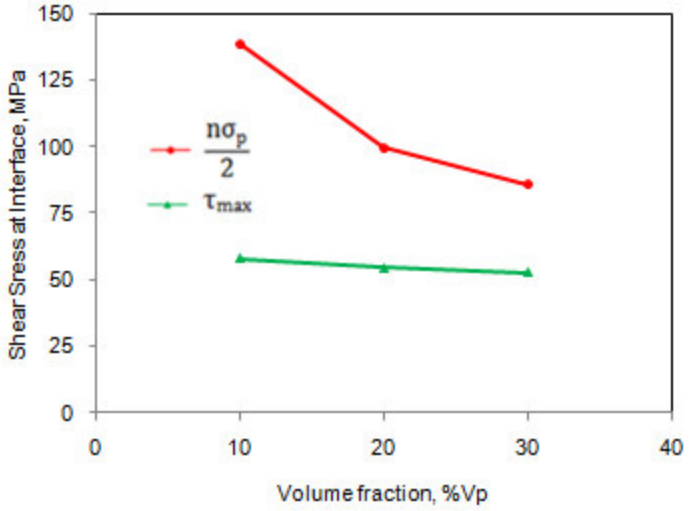


**Figure 3:** Fracture criteria of interface debonding.

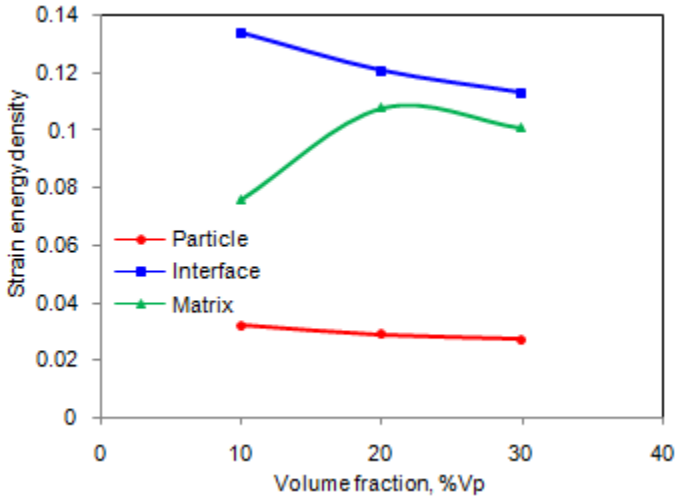


**Figure 4:** Effect of volume fraction on strain energy density.

The normal and tangential tractions are plotted in figure 6. Because of symmetry considerations, the variations of the interface stresses with circumferential location are plotted only for the range $0^o \leq \theta \leq 90^o$. The tractions stresses were calculated locally near the interface. The normal traction in the region of interface between graphite nanoparticle and AA1100 alloy matrix decreases with increase of volume fraction of graphite. When the normal and tangential tractions are tensile the separation takes place between graphite nanoparticle and AA1100 alloy matrix. When these are compressive in nature, the AA1100 alloy matrix adheres to the graphite nanoparticle. The interfacial debonding continues along the graphite nanoparticle periphery till

the normal traction becomes zero. The separation was high in the composites having 20% graphite and it is least in the composites comprising 30%graphite nanoparticles. The normal displacement becomes zero between 45° - 55° along the interface. The plots shown in figure 6 represent the normal traction dominated failure because of tensile loading. The raster images of interfacial debonding are shown in figure 7. Apart from the interfacial debonding, the graphite nanoparticle experiences high stress due to load transfer from the matrix to it. The stress induced was high in the composites having 30%graphite nanoparticles. The scanning electron microscopy image indicates clearly the interfacial debonding in the composites having 30%grpahite.

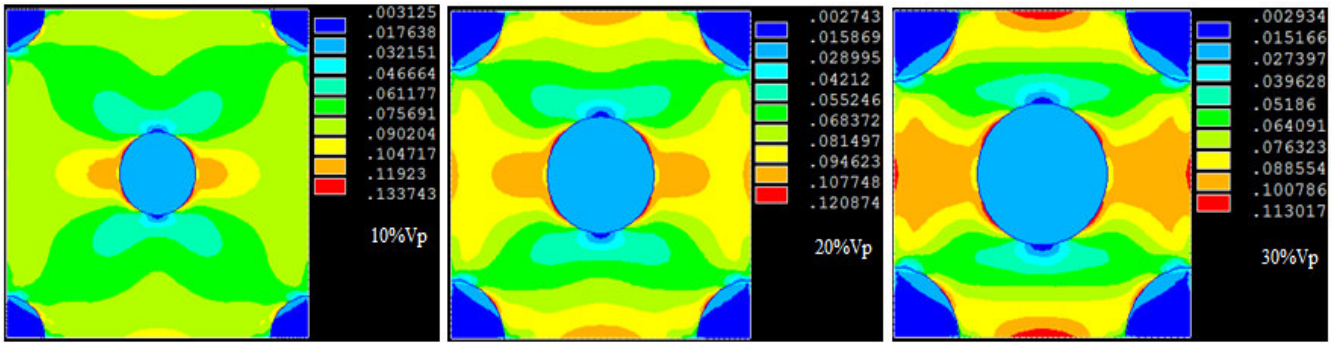


**Figure 5:** FEA results of strain energy densities.

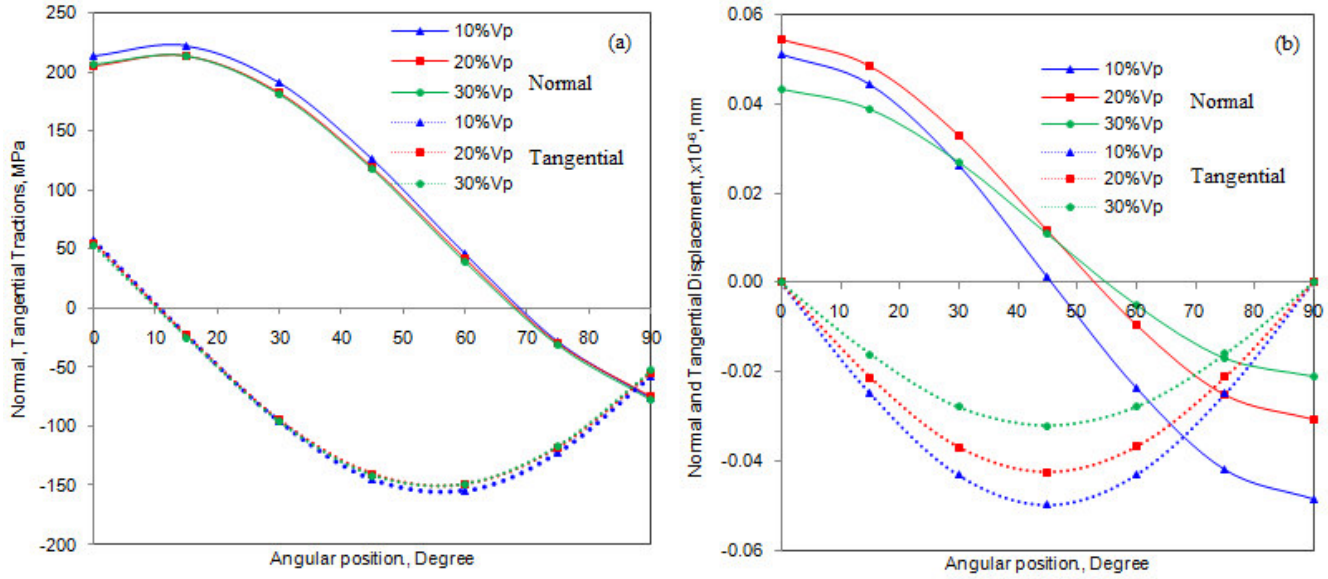


**Figure 6:** Normal and tangential: (a) tractions and (b) displacements.

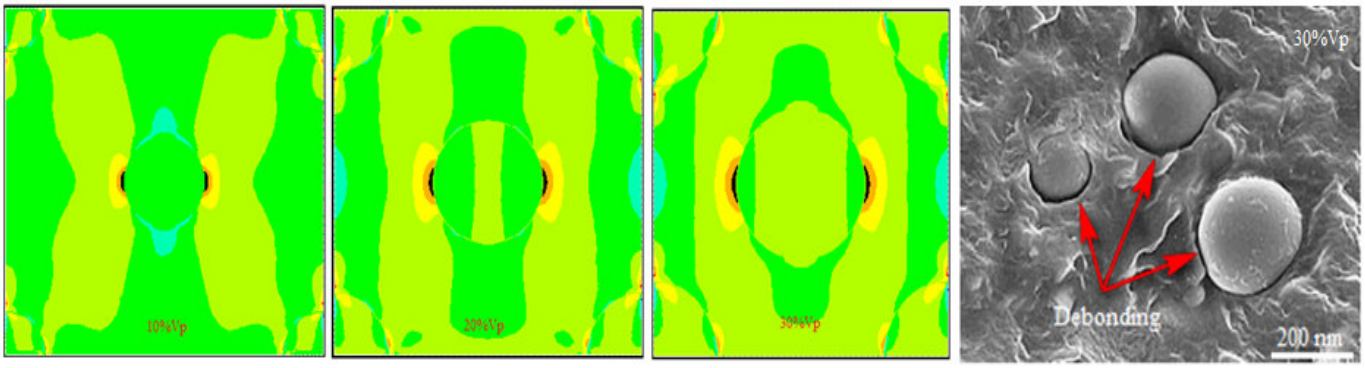


**Figure 7:** Interfacial debonding.

## 2. CONCLUSION

The interface debonding occurred in the composites containing 10%, 20% and 30% volume fractions graphite. When the normal and tangential tractions are tensile the separation takes place between graphite nanoparticle and AA1100 alloy matrix. he normal displacement becomes zero between $45^o$ - $55^o$ along the interface. In addition to interfacial debonding, the graphite nanoparticle experiences high stress due to load transfer from the matrix.

## REFERENCES

1. Y. Wu, E. J. Lavernia, Strengthening behavior of particulate reinforced MMCs, Scripta Materialia, 27, 1992, pp.173–178.
2. A. Needleman, Micromechanical Modelling of Interfacial Decohesion" Ultramicroscopy, 40(3), 1992, pp. 203–214.
3. M. E. Gurtin, An Introduction to Continuum Mechanics, Academic Press, New York, 1981.
4. A. Chennakesava Reddy, Assessment of Debonding and Particulate Fracture Occurrences in Circular Silicon Nitride Particulate/AA5050 Alloy Metal Matrix Composites , National Conference on Materials and Manufacturing Processes, Hyderabad, India, 27-28 February1998, pp.104-109.
5. B. Kotiveera Chari and A. Chennakesava Reddy, Numerical Simulation of Particulate Fracture in Round Silicon Nitride Particulate/AA6061 Alloy Metal Matrix Composites, National Conference on Materials and Manufacturing Processes, Hyderabad, India, 27-28 February 1998, pp. 110-114.
6. H. B. Niranjan and A. Chennakesava Reddy, Effect of Elastic Moduli Mismatch on Particulate Fracture in AA7020/Silicon Nitride Particulate Metal Matrix Composites , National Conference on Materials and Manufacturing Processes, Hyderabad, India, 27-28 February, 1998, pp. 115-118,
7. P. Martin Jebaraj and A. Chennakesava Reddy, Cohesive Zone Modelling for Interface Debonding in AA8090/Silicon Nitride Nanoparticulate Metal Matrix Composites, National Conference on Materials and Manufacturing Processes, Hyderabad, India, 27-28 February 1998, pp. 119-122.
8. P. Martin Jebaraj and A. Chennakesava Reddy, Plane Strain Finite Element Modeling for Interface Debonding in AA1100/Silicon Oxide Nanoparticulate Metal Matrix Composites, National Conference on Materials and Manufacturing Processes, Hyderabad, India, 27-28 February 1998, pp. 123-126.
9. A. Chennakesava Reddy, Local Stress Differential for Particulate Fracture in AA2024/Titanium Carbide Nanoparticulate Metal Matrix Composites, National Conference on Materials and Manufacturing Processes, Hyderabad, India, 27-28 February 1998, pp. 127-131.
10. B. Kotiveera Chari and A. Chennakesava Reddy, Interface Debonding and Particulate Facture based on Strain Energy Density in AA3003/MgO Nanoparticulate Metal Matrix Composites, National Conference on Materials and Manufacturing Processes, Hyderabad, India, 27-28 February 1998, pp. 132-136.
11. H. B. Niranjan and A. Chennakesava Reddy, Numerical and Analytical Prediction of Interface Debonding in AA4015/Boron Nitride Nanoparticulate Metal Matrix Composites , National Conference on Materials and Manufacturing Processes, Hyderabad, India, 27-28 February 1998, pp. 137-140.
12. S. Sundara Rajan and A. Chennakesava Reddy, Effect of Particulate Volume Fraction on Particulate Cracking in AA5050/Zirconium Oxide Nanoparticulate Metal Matrix Composites , National Conference on Materials and Manufacturing Processes, Hyderabad, India, 27-28 February 1998, pp. 156-159.
13. S. Sundara Rajan and A. Chennakesava Reddy, Cohesive Zone Analysis for Interface Debonding in AA6061/Titanium Nitride Nanoparticulate Metal Matrix Composites , National Conference on Materials and Manufacturing Processes, Hyderabad, India, 27-28 February 1998, pp. 160-164.
14. A. Chennakesava Reddy, Effect of Particle Loading on Microealstic Behavior and interfacial Tractions of Boron Carbide/AA4015 Alloy Metal Matrix Composites, 1st International Conference on Composite Materials and Characterization, Bangalore, 14-15 march 1997, pp. 176-179.7
15. A. Chennakesava Reddy, Reckoning of Micro-stresses and interfacial Tractions in Titanium Boride/AA2024 Alloy Metal Matrix Composites, 1st International Conference on Composite Materials and Characterization, Bangalore, 14-15 march 1997, pp. 195-197.
16. A. Chennakesava Reddy, Interfacial Debonding Analysis in Terms of Interfacial Tractions for Titanium Boride/AA3003 Alloy Metal Matrix Composites, 1st National Conference on Modern Materials and Manufacturing , Pune, India, 19-20 December 1997, pp. 124-127.
17. A. Chennakesava Reddy, Evaluation of Debonding and Dislocation Occurrences in Rhombus Silicon Nitride Particulate/AA4015 Alloy Metal Matrix Composites, 1st National Conference on Modern Materials and Manufacturing , Pune, India, 19-20 December 1997, pp. 278-282.